Heliyon

ELSEVIER

Received:
22 June 2016
Revised:
14 September 2016
Accepted:
10 October 2016

Heliyon 2 (2016) e00178

Frequency domain model for transient analysis of lightning protection systems of buildings

Pablo Gómez

Deparment of Electrical and Computer Engineering, Western Michigan University, Kalamazoo, MI 49008, United States

E-mail address: pablo.gomez@wmich.edu (P. Gómez).

Abstract

A frequency domain modeling approach for lightning protection systems (LPS) of buildings is described and validated in this paper. The model is based on a 2-port transmission line representation of each conductor, and the further assembling of a network representing the complete structure. Horizontal and vertical conductors are modeled using formulas based on the complex images method, in order to take into account frequency dependence. Variation of electrical parameters with height is also considered for vertical conductors. This is accomplished by means of a non-uniform modeling approach based on conductor subdivision and cascaded connection of chain matrices computed for each segment. The results from the model are validated by means of comparisons with measurements reported elsewhere, as well as simulations using PSCAD/EMTDC.

Keywords: Electromagnetism, Engineering

1. Introduction

The objective of lightning protection systems (LPS) of buildings is the dissipation of lightning currents to ground with the least possible impact on equipment, installations and people inside the building. This impact is mostly due to the electromagnetic environment (conducted and radiated fields) generated by the circulating currents from the point of impact of the lightning stroke to the grounding electrodes [1]. Large voltage differences between different points of the structure, which are dangerous to persons and equipment inside the building, can

http://dx.doi.org/10.1016/j.heliyon.2016.e00178

also appear as a result of the circulating currents. Electronic and communication components (sensitive equipment) are particularly prone to damage or failure under this conditions. In addition, the performance of LPS structures is especially important when photovoltaic (PV) modules are installed on building roofs [2].

LPS are formed of metallic components in reinforced concrete or steel constructions, as well as vertical and horizontal conductors located outside of the structure, similarly to a Faraday cage [3]. An example is shown in Fig. 1.

Transient analysis of LPS struck by direct lightning strokes can be performed by means of field measurements or experimental setups on reduced-scale prototypes [1], [3], as well as digital simulations using different software tools. Experimental tests are usually complicated, expensive and case sensitive. On the other hand, simulations can deal with different test cases in a simpler manner.

There are several approaches for the simulation of building structure arrangements, such as those based on equivalent lumped-parameter circuits [4, 5, 6, 7], method of moments, [8, 9, 10], finite-difference-time-domain method (FDTD) [11, 12, 13, 14], finite element method (FEM) [15], [16], etc. An alternative approach is the representation of the structure by means of a network consisting of horizontal and vertical transmission lines. This has been previously applied to tower modeling with very good results [17], [18].

In this work, a frequency domain model of the LPS for direct lightning studies is described. This model is based on the representation of each horizontal or vertical

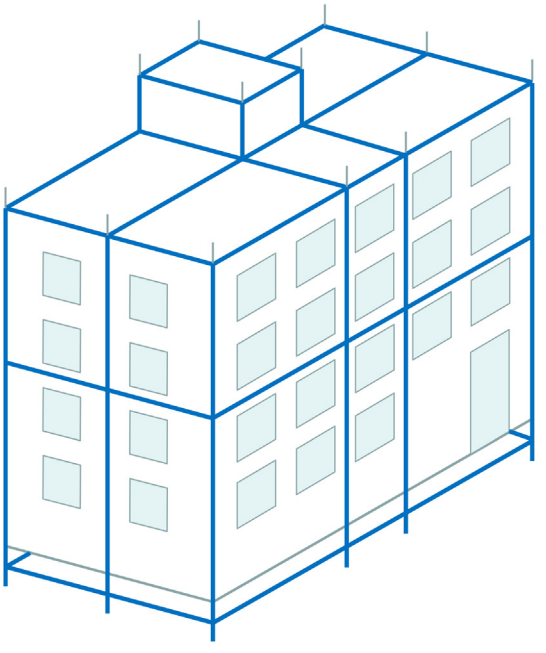

Fig. 1. Lightning protection structure of a building.

http://dx.doi.org/10.1016/j.heliyon.2016.e00178

structure component by means of a 2-port transmission line model. Once all of the components are modeled, an admittance matrix model for the complete structure is defined, which is then solved for the nodal voltages. From such voltages, the current circulating along each structure component is also computed. Finally, the time domain response of the structure is obtained applying the inverse numerical Laplace transform [19].

The results from the proposed model are compared with experimental results reported in [3], as well as results from a model implemented in the professional software PSCAD/EMTDC.

The contributions of this work can be summarized as follows:

1. The proposed model considers frequency dependence of the structure components due to skin effect in conductors and finite ground conductivity, as well as non-uniformity of the vertical conductors parameters, due to variation with height.
2. It is demonstrated that the computation of transient overvoltages at different nodes of the LPS structure requires an accurate modeling of both horizontal and vertical conductors, considering frequency dependence and non-uniformity (in the case of vertical components). This is not possible with the current capabilities of existing transient simulation programs. PSCAD/EMTDC is used for comparisons, but other EMTP-type programs have the same limitations for vertical conductor modeling.
3. It is also demonstrated that the circulating currents along the structure can be obtained with sufficient accuracy with a professional simulation software (PSCAD/EMTDC), using existing transmission line models.

The inductive and capacitive coupling between structure components is neglected in this work, aiming at a balance between accuracy and practicality of the modeling proposal. Simulation results show that, for the test cases under consideration, this coupling is not a significant parameter, since the difference between simulation and experimental results are below 5% in average. This is due to the fact that the distance between conductors is equal to or larger than their length for all of the structure components, resulting in a low coupling factor. This observation is very important because a single conductor based model is simpler, less computer-time consuming and easier to implement in a commercial software package than a multiconductor based model. Bearing in mind that for LPS the transversal distance between conductors is oftentimes comparable to the lengths of the structure elements, the model described in the paper can be applied with enough confidence for a variety of real cases. Nonetheless, future work will explore the application of a multiconductor transmission line modelling approach to consider more general cases which may not comply with this and could present larger coupling factors.

http://dx.doi.org/10.1016/j.heliyon.2016.e00178

2. Model

There are 3 fundamental components of the LPS model:

1. Horizontal conductors
2. Vertical conductors
3. Grounding components

The modeling approach followed for each component is described below.

2.1. Horizontal conductors

Each of the horizontal conductors in the metallic structure is modeled similarly to an aerial single-phase line. The model starts from the telegrapher equations in the frequency domain for a single conductor. Applying boundary conditions, the 2-port representation (admittance matrix) used in this work is obtained:

$$\begin{bmatrix} I_L \\ I_R \end{bmatrix} = \begin{bmatrix} A_h & -B_h \\ -B_h & A_h \end{bmatrix} \begin{bmatrix} V_L \\ V_R \end{bmatrix} \tag{1}$$

where V_L, V_R I_L e I_R, are the nodal voltages and currents at the left and right ends of the conductor, respectively. Admittance matrix elements of a horizontal conductor are defined as

$$A_h = \sqrt{\frac{Y_h}{Z_h}} \coth\left(\sqrt{Z_h Y_h}\ell_h\right) \tag{2a}$$

$$B_h = \sqrt{\frac{Y_h}{Z_h}} \operatorname{csch}\left(\sqrt{Z_h Y_h}\ell_h\right) \tag{2b}$$

where Z_h and Y_h are the series impedance and shunt admittance of the horizontal conductor, respectively, and ℓ_h is its length. Parameter computation for horizontal conductors is well-known [20] and is only summed up in the remaining of this section for completeness of the paper.

Series impedance of a bare horizontal conductor can be divided in 3 parts: geometrical impedance, $Z_{h,G}$, impedance do to the finite ground conductivity, $Z_{h,E}$, and internal conductor impedance, $Z_{h,C}$:

$$Z_h = Z_{h,G} + Z_{h,E} + Z_{h,C} \tag{3}$$

Geometric impedance is computed considering perfectly conducting ground and applying the method of images. This yields the following expression:

$$Z_{h,G} = \frac{j\omega\mu_0}{2\pi} \ln\left(\frac{2h}{r}\right) \tag{4}$$

where ω is the angular frequency, μ_0 is the permeability of free space, h is the conductor height above ground and r is its radius.

http://dx.doi.org/10.1016/j.heliyon.2016.e00178

Impedance due to finite ground conductivity is computed applying the method of complex images [21], [22]. It is considered that the ground return current is limited by a fictitious plane parallel to the earth plane and given by a complex penetration depth, p, defined as

$$p = \frac{1}{\sqrt{j\omega\mu_0\sigma_E}} \tag{5}$$

where σ_E is the ground conductivity. From this definition, the impedance component of the horizontal conductor due to the finite ground conductivity is given by

$$Z_{h,E} = \frac{j\omega\mu_0}{2\pi}\ln\left(1+\frac{p}{h}\right) \tag{6}$$

Internal conductor impedance is due to skin effect, this is, the tendency of current to concentrate in the conductor' surface as frequency increases. This phenomenon is approximated by means of the concept of complex penetration depth inside the conductor, δ, expressed as

$$\delta = \frac{1}{\sqrt{j\omega\mu_0\sigma_C}} \tag{7}$$

where σ_E is the conductivity of the conductor. Considering both dc and high frequency components of the internal impedance, the following expression is obtained:

$$Z_{h,C} = \frac{\sqrt{4\delta^2 + r^2}}{2\pi r^2\sigma_C\delta} \tag{8}$$

On the other hand, shunt admittance of a horizontal conductor is also computed from the method of images; the corresponding expression is

$$Y_h = \frac{j\omega 2\pi\varepsilon_0}{\ln\left(\frac{2h}{r}\right)} \tag{9}$$

2.2. Vertical conductors

Parameter computation of vertical conductors follows the approach proposed by Gutiérrez et al. for tower modeling [17]. In this reference, a vertical conductor is represented by means of a non-uniform line, considering that its electrical parameters are a function of the vertical position. Therefore, each vertical conductor is divided into n segments, computing the electrical parameters of each segment. In [17], the resulting system is solved using the method of characteristics, a finite differences method for time-domain solution of the telegrapher equations. Conversely, in this work the frequency domain chain matrix model of each segment is obtained, and then the method of chain connection of chain matrices is

http://dx.doi.org/10.1016/j.heliyon.2016.e00178

applied, as described in [18]. With this method, a chain matrix model for the complete vertical conductor is obtained as follows:

$$\begin{bmatrix} V_U \\ I_U \end{bmatrix} = \mathbf{\Phi}_n \mathbf{\Phi}_{n-1} \ldots \mathbf{\Phi}_2 \mathbf{\Phi}_1 \begin{bmatrix} V_D \\ I_D \end{bmatrix} = \mathbf{\Phi}_V \begin{bmatrix} V_D \\ I_D \end{bmatrix} \tag{10}$$

where V_U, V_D, I_U and I_D are the voltages and currents at the upper and lower ends of the vertical conductor, respectively;$\mathbf{\Phi}_v$ is the chain matrix of the complete conductor, and $\mathbf{\Phi}_i$ is the chain matrix of the i-th vertical conductor, defined as

$$\mathbf{\Phi}_i = \begin{bmatrix} \cosh\left(\sqrt{Z_v^i Y_v^i}\ell_v/n\right) & -\sqrt{\frac{Z_v^i}{Y_v^i}}\sinh\left(\sqrt{Z_v^i Y_v^i}\ell_v/n\right) \\ -\sqrt{\frac{Y_v^i}{Z_v^i}}\sinh\left(\sqrt{Z_v^i Y_v^i}\ell_v/n\right) & \cosh\left(\sqrt{Z_v^i Y_v^i}\ell_v/n\right) \end{bmatrix} \tag{11}$$

where Z_v^i and Y_v^i are the electrical parameters (series impedance and shunt admittance) of the i-th segment of the vertical conductor, ℓ_V is the length of the complete conductor and n is the number of subdivisions.

Series impedance of the i-th segment of the vertical conductor, Z_i, is computed considering that this parameter is formed by 3 components, similarly to the expression given by Eq. (3) for horizontal conductors:

$$Z_v^i = Z_{v,G}^i + Z_{v,E}^i + Z_{v,C}^i \tag{12}$$

The corresponding formulas are [17]:

$$Z_{v,G}^i = \frac{j\omega\mu_0}{2\pi}\ln\left(\frac{\sqrt{h_i^2 + r^2} + h_i}{r}\right) \tag{13a}$$

$$Z_{v,E}^i = \frac{j\omega\mu_0}{2\pi}\ln\left(\frac{\sqrt{(h_i + p)^2 + r^2} + h_i + p}{\sqrt{h_i^2 + r^2} + h_i}\right) \tag{13b}$$

where h_i is the height of the i-th conductor segment. Internal impedance of each segment of the vertical conductor, $Z_{v,C}^i$, is computed applying the same equation used for horizontal components [Eq. (8)].

On the other hand, the shunt admittance of the i-th segment of the vertical conductor, Y_v^i, is computed as

$$Y_v^i = \frac{j\omega 2\pi\varepsilon_0}{\ln\left(\frac{\sqrt{h_i^2+r^2}+h_i}{r}\right)} \tag{14}$$

Once the chain matrix of the complete vertical conductor is computed according to Eqs. (10) and (11), it is transformed into an admittance matrix, so that it can be directly used (in conjunction with Eq. (1)) to assemble the network of horizontal

http://dx.doi.org/10.1016/j.heliyon.2016.e00178

and vertical conductors representing the building structure, as described in Section 2.4. In order to perform such transformation, Eq. (10) is rewritten in terms of the elements of the chain matrix of the vertical conductor:

$$\begin{bmatrix} V_U \\ I_U \end{bmatrix} = \begin{bmatrix} \Phi_{11} & \Phi_{12} \\ \Phi_{21} & \Phi_{22} \end{bmatrix} \begin{bmatrix} V_D \\ I_D \end{bmatrix} \tag{15}$$

By means of a simple algebraic manipulation of Eq. (15) an admittance matrix model of the vertical conductor is obtained [23]:

$$\begin{bmatrix} I_D \\ I_U \end{bmatrix} = \begin{bmatrix} -\Phi_{12}^{-1}\Phi_{11} & \Phi_{12}^{-1} \\ \Phi_{22}\Phi_{12}^{-1}\Phi_{11} - \Phi_{21} & -\Phi_{22}\Phi_{12}^{-1} \end{bmatrix} \begin{bmatrix} V_D \\ V_U \end{bmatrix} = \begin{bmatrix} A_v & -B_v \\ -B_v & A_v \end{bmatrix} \begin{bmatrix} V_D \\ V_U \end{bmatrix} \tag{16}$$

2.3. Grounding components

Dissipation of lightning currents to ground is done by means of buried metallic electrodes (ground rods). These electrodes can be included in the LPS model in 3 different ways:

1. As simple footing resistances.
2. As lumped-parameter RLC circuits representing each vertical electrode.
3. By means of distributed-parameter representations which consider the propagation along the rods. The dependence of parameters on the vertical position (non-uniform model) can also be accounted for.

Any of these representations can be included in the proposed model. If the third option is considered (including the non-uniformity of electrical parameters), the ground rod model will be very similar to the model described for vertical conductors of the building structure. The main difference lies in the computation of the shunt admittance. For ground rods, this parameter has to include, besides the capacitive component, a shunt conductance component through which the lightning current is dissipated to ground [24]. The corresponding expression is as follows (modified from [17]):

$$Y_{gr}^{i} = \frac{2\pi(\sigma_E + j\omega\varepsilon_E)}{ln\left(\frac{\sqrt{h_i^2+r^2}+h_i}{r}\right)} \tag{16b}$$

where ε_E is the ground permittivity. Also, in this case h_i represents the vertical position of the i-th segment of the rod in the $-y$ direction (instead of the $+y$ direction as in Eq. (14)).

2.4. Network assembly and frequency domain solution

Considering a system consisting of N nodes, the complete metallic structure is described by means of a nodal or admittance matrix model as follows:

http://dx.doi.org/10.1016/j.heliyon.2016.e00178

$$\begin{bmatrix} I_1 \\ I_2 \\ \vdots \\ I_N \end{bmatrix} = \begin{bmatrix} Y_{11} & Y_{12} & \cdots & Y_{1N} \\ Y_{21} & Y_{22} & \cdots & Y_{2N} \\ \vdots & \vdots & \ddots & \vdots \\ Y_{N1} & Y_{N2} & \cdots & Y_{NN} \end{bmatrix} \begin{bmatrix} V_1 \\ V_2 \\ \vdots \\ V_N \end{bmatrix} \tag{17}$$

where Y_{ij} is the element located at row i and column j of the structure admittance matrix, I_i is the i-th element of the injection currents vector, and V_i is the i-th element of the nodal voltages vector. Insertion of a structure component (horizontal or vertical) between nodes i and j of the admittance matrix defined in Eq. (17) modifies such matrix according to

$$\begin{bmatrix} Y_{ii} & \cdots & Y_{ij} \\ \vdots & \ddots & \vdots \\ Y_{ji} & \cdots & Y_{jj} \end{bmatrix}_{new} = \begin{bmatrix} Y_{ii} & \cdots & Y_{ij} \\ \vdots & \ddots & \vdots \\ Y_{ji} & \cdots & Y_{jj} \end{bmatrix}_{old} + \begin{bmatrix} A & \cdots & -B \\ \vdots & \ddots & \vdots \\ -B & \cdots & A \end{bmatrix} \tag{18}$$

where A and B are the elements of the admittance matrix of a single structure component, defined by Eqs. (2a) and (2b) for horizontal components and by Eq. (16) for vertical components. Subscripts "old" and "new" indicate the elements of the admittance matrix before and after the insertion of the structure component. Application of Eq. (18) is repeated for each existing component until the network representing the metallic structure is formed, as defined in Eq. (17). This equation is solved for the nodal voltages, considering the lightning current excitation at the corresponding node (point of impact) by means of the injection currents vector. Inclusion of lumped-parameter elements (for example footing resistances), is performed similarly to Eq. (18).

Finally, the current circulating between nodes i and j is computed according to

$$I_{ij} = Y_{ij}\left(V_j - V_i\right) \tag{19}$$

Time domain response of the structure is obtained by means of the inverse numerical Laplace transform [19].

3. Results

In order to validate the results from the model presented in this work, two test cases taken from [3] are considered. This reference presents experimental measurements (reduced-scale) of the current distribution within industrial building structures. The arrangements used for model validation are reproduced in Fig. 2. Hereafter, arrangements from Fig. 2(a) and (b) are denoted as structure A and structure B, respectively. Both structures consist of horizontal and vertical steel conductors. The dimensions of each structure are shown in Fig. 2. For the experimental setups under consideration, the structures are not grounded by means of vertical rods but instead by simple low resistances. In addition [3], does not mention the values of such resistances for the structures considered for validation; therefore, a value of 2 Ω was assumed for the simulations. Ground resistivity and conductors' radius are

http://dx.doi.org/10.1016/j.heliyon.2016.e00178

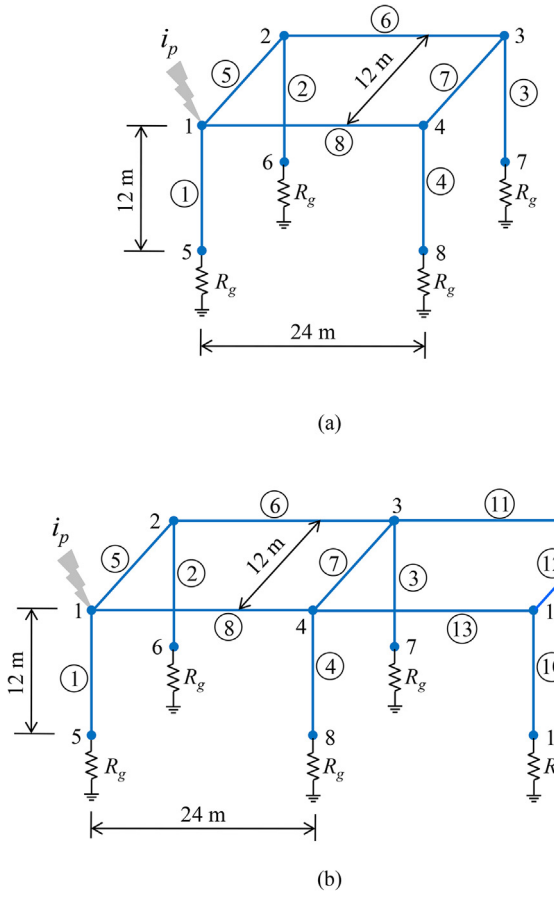

Fig. 2. Structures considered for validation of the proposed model: a) structure A, b) structure B [3].

not mentioned either, thus a resistivity of 100 Ω-m (typical for most cases) and a radius of 1 mm (remembering that this is a reduced-scale test) are assumed. Wave-shape of the lightning current (i_p in Fig. 2) used for experimental tests and simulations, is given by the following expression [1]:

$$i(t) = \Sigma_{i=1}^{n} t^{\delta_i} A_i e^{-\alpha_i t} \tag{20}$$

with $n = 4$. The remaining values used in Eq. (20) are listed in Table 1.

Table 1. Parameters of the lightning current wave-shape [1].

n	A (A/μs^2)	δ (dimensionless)	α (1/μs)
1	100500	2	0.99
2	390	2	0.063
3	2100	2	0.18
4	14500	2	0.4

http://dx.doi.org/10.1016/j.heliyon.2016.e00178

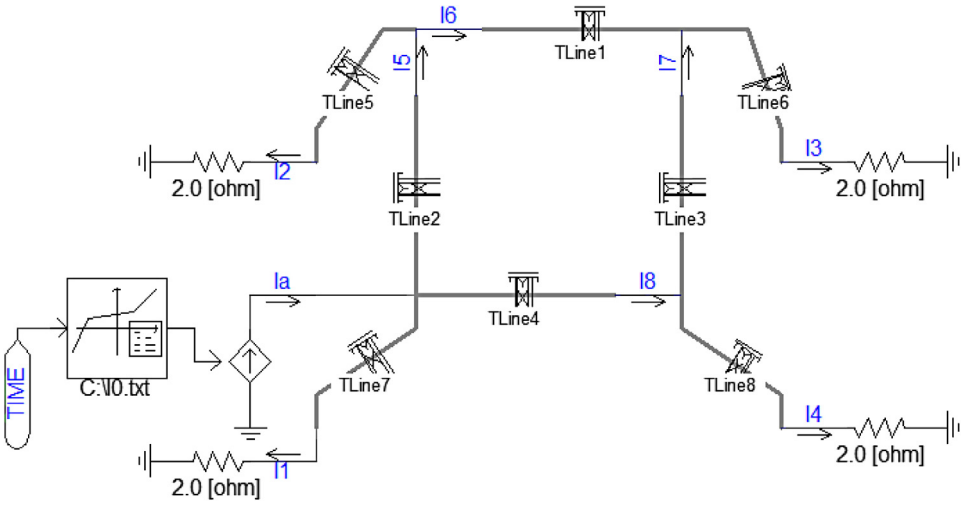

Fig. 3. Structure A implemented in PSCAD/EMTDC.

Additionally, the structures shown in Fig. 2 were modeled using the professional software PSCAD/EMTDC v.4.5. As an example, Fig. 3 shows the implementation of structure A. In this software, horizontal elements were represented by single-phase lines using the frequency-dependent line model denoted in this program as "Phase domain model" [25]. However, this software does not include models for vertical conductors. Therefore, such conductors were modeled using the constant-parameter Bergeron model [26], and computing their characteristic impedances according to the expression proposed by Hara for vertical conductors [27]:

$$Z_0 = 60\left[\ln\left(\frac{2\sqrt{2}h}{r}\right) - 2\right] \tag{21}$$

This formula has shown good results with respect to lab tests [28] and simulations using FEM [29]. However, it does not consider the non-uniform and frequency dependent nature of electrical parameters for vertical conductors.

3.1. Results for structure A

Fig. 4 shows the transient current obtained at different conductors (branches) of structure A, comparing the results obtained with the proposed model (hereafter denoted as FD model) from those obtained using PSCAD/EMTDC. It can be noticed that the responses from both methods are very similar. Then, the maximum current values at each conductor of the structure are computed and compared to the experimental results reported in [3]. This is shown in Table 2. Branch numbering can be identified in Fig. 2(a). Additionally, relative differences between simulation results and experimental measurements are computed. This is shown in Fig. 5.

http://dx.doi.org/10.1016/j.heliyon.2016.e00178

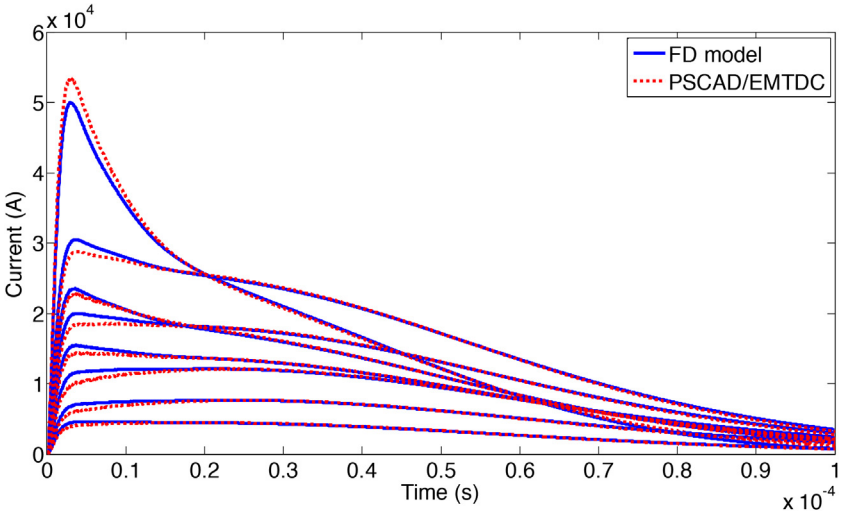

Fig. 4. Transient currents at different branches of structure A.

It can be observed that the relative difference of the proposed model against measurements remains below 10% for all of the branches, while in PSCAD/EMTDC it reaches a value of 17.36% at branch 1, and exceeds 10% at 3 of the 8 branches. Besides, the average relative difference of the proposed model is considerably lower than that of PSCAD/EMTDC (4.65% vs 8.33%).

In addition to the circulating current, another important parameter to be evaluated is the voltage at different nodes of the structure. A large potential difference can be dangerous to people and equipment inside the building. Fig. 6 shows the transient overvoltages produced by the lightning stroke at nodes 1 to 4 of the structure (node numbering is shown in Fig. 2(a)). The results obtained with PSCAD/EMTDC are also included. Unlike the circulating currents, the transient overvoltages computed by both methods are clearly different, particularly in terms of amplitude.

Table 2. Maximum current value at different branches of structure A.

Branch	**max[$i(t)$]**		
	Measurement from [3]	**FD model**	**PSCAD/EMTDC**
1	45600	49993.62	53517.44
2	23250	23539.57	22829.80
3	12710	12105.69	12104.51
4	16500	15481.07	14458.61
5	31500	30478.90	28784.32
6	8000	7666.99	7656.40
7	4750	4592.83	4473.65
8	21000	20010.30	18558.37

http://dx.doi.org/10.1016/j.heliyon.2016.e00178

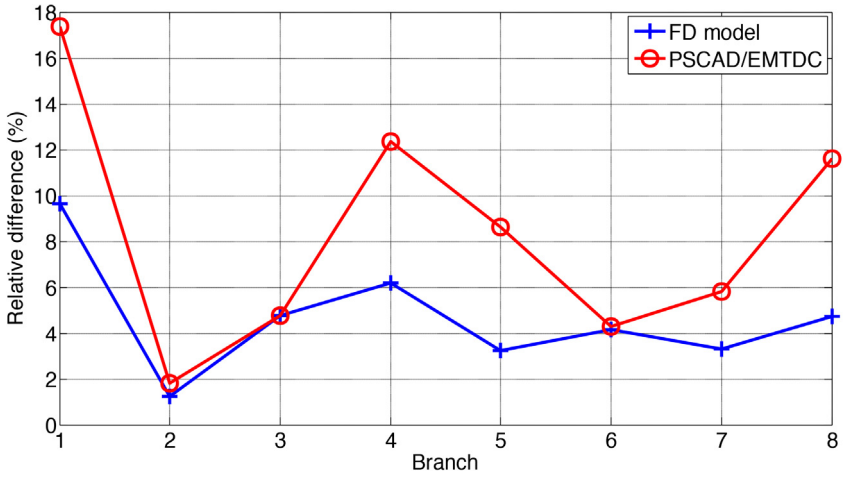

Fig. 5. Relative differences between the results from simulations and experimental measurements for structure A.

To explore the reasons for these differences, Fig. 7 shows the frequency spectrum of the characteristic impedance magnitude of a typical vertical element (notice that structures A and B have the same type of vertical elements). This spectrum is compared with the constant value of characteristic impedance applied for PSCAD/EMTDC simulations. The following remarks are obtained from this figure:

1. For a large part of the frequency spectrum, the characteristic impedance computed for the vertical conductors of the proposed model is larger than the value used in PSCAD/EMTDC. This results in larger overvoltage magnitudes, since the magnitude of the voltage traveling-wave is directly proportional to the characteristic impedance of the conductor.

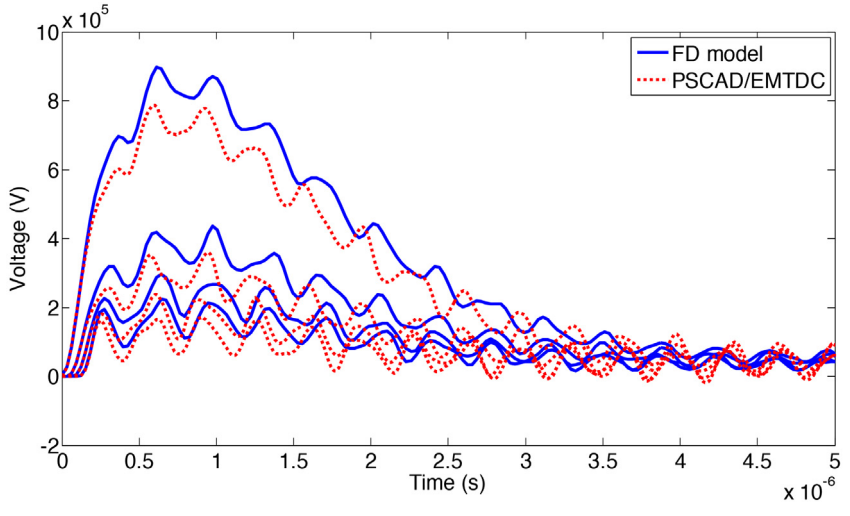

Fig. 6. Transient overvoltages at nodes 1 to 4 of structure A.

http://dx.doi.org/10.1016/j.heliyon.2016.e00178

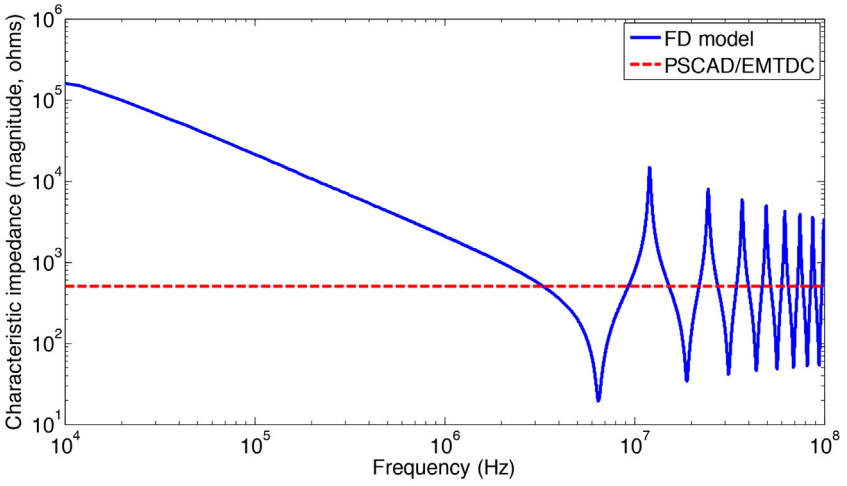

Fig. 7. Frequency spectrum of the characteristic impedance magnitude for a typical vertical conductor of structures A or B.

2. In the high frequency region, the frequency spectrum of the characteristic impedance computed for the vertical conductors of the proposed model is highly oscillatory. These resonances are not considered in the characteristic impedance introduced into PSCAD/EMTDC. In consequence, differences in phase and frequency content can be noticed in the transient overvoltages obtained by both computational methods.

To sum up, the simulations obtained with PSCAD/EMTDC underestimate the overvoltages at different nodes of the structure. This can result in an insufficient protection of people and equipment inside the building.

3.2. Results for structure B

Fig. 8 shows the transient current circulating along different conductors of structure B. Similarly to the previous case, it can be seen that the responses from the proposed model and PSCAD/EMTDC are very similar. The maximum current values at each conductor of the structure are computed and compared with the measurements from [3]. This is listed in Table 3. Relative difference between simulations and experimental results are shown in Fig. 9.

Although in this case the results from PSCAD/EMTDC at some branches are slightly closer to the measurements than the results from the proposed model, the average relative difference of the proposed model is lower than the one obtained with PSCAD/EMTDC (4.37% vs 4.80%). Besides, the relative difference between the proposed model and the measurements remains below 10% for all of the branches. This is not the case for the PSCAD/EMTDC results: the relative difference with respect to measurements reaches 17.24% % at branch 1.

http://dx.doi.org/10.1016/j.heliyon.2016.e00178

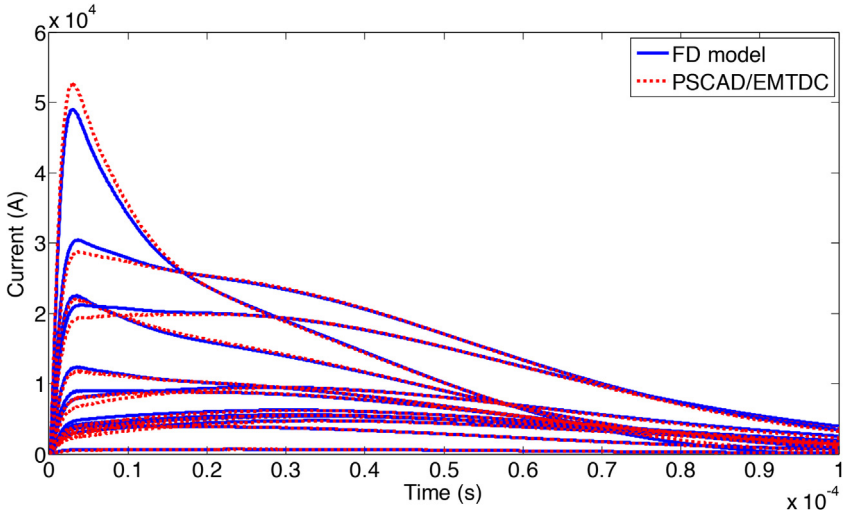

Fig. 8. Transient currents at different branches of structure B.

Finally, Fig. 10 shows the transient overvoltages at nodes 1 to 4 of structure B. The results are similar to those obtained for structure A: waveforms are significantly different in amplitude, presenting also differences in phase and frequency content. This supports the conclusion obtained from the previous case, regarding the necessity of including the frequency dependence and non-uniformity of vertical conductors' parameters in order to avoid underestimating overvoltages at the structure nodes.

Table 3. Maximum current value at different branches of structure B.

Branch	max[$i(t)$]		
	Measurement from [3]	**FD model**	**PSCAD/EMTDC**
1	45000	48959.87	52757.83
2	22000	22521.83	22077.25
3	8380	9020.12	8819.80
4	11800	12383.68	11789.18
5	31250	30404.74	28723.81
6	9000	9491.77	9417.56
7	4000	4059.40	3901.14
8	22000	21197.84	19865.75
9	5130	5407.44	5353.06
10	5500	5577.47	5516.27
11	4340	4750.28	4692.43
12	690	678.39	683.47
13	6130	6244.15	6181.05

http://dx.doi.org/10.1016/j.heliyon.2016.e00178

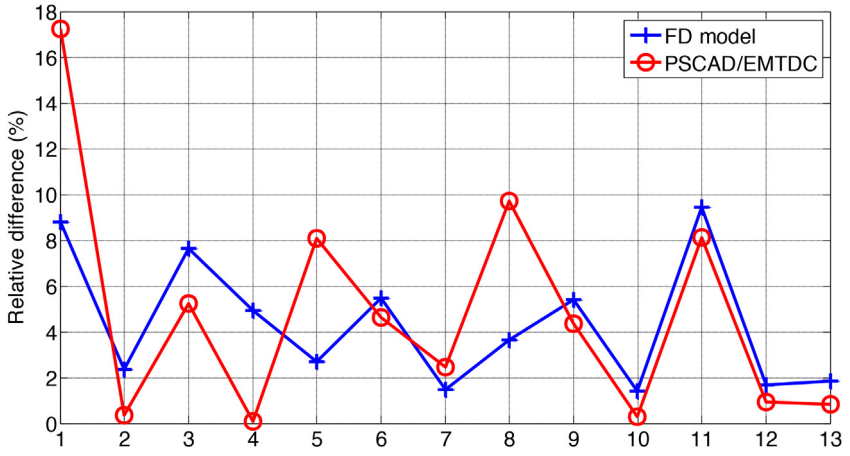

Fig. 9. Relative differences between the results from simulations and experimental measurements for structure B.

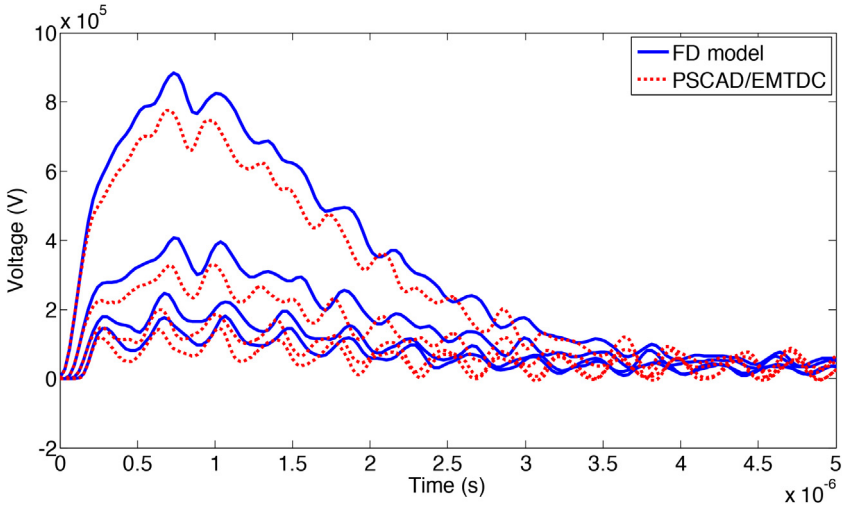

Fig. 10. Transient overvoltages at nodes 1 to 4 of structure B.

4. Conclusions

The modeling of metallic structures for lightning protection of buildings has been described and evaluated in this work. The proposed model is based on representing the horizontal and vertical components of the structures by means of transmission lines in the frequency domain.

By means of two test cases, it is demonstrated that the proposed model yields very good results with respect to experimental measurements, maintaining a relative difference below 10% for all of the structure branches, and an average relative difference below 5%.

http://dx.doi.org/10.1016/j.heliyon.2016.e00178

Both test cases were also implemented using the professional software PSCAD/EMTDC. According to the results, the currents circulating along the structure can be computed with good accuracy with this software tool. This is due to the fact that the potential difference between terminal nodes of each conductor is also computed with accuracy. However, the overvoltages at different nodes of the structure are substantially underestimated. The reason for this is that PSCAD/EMTDC does not include detailed models of vertical conductors; thus, they have to be approximated by means of simple Bergeron representations, which do not consider frequency dependence and non-uniformity of their electrical parameters.

The frequency domain model proposed here can be used as a standalone tool for accurate computation of the transient response of lightning protection structures of buildings or as base solution for future implementation of time domain models using commercial software tools.

The application of numerical methods based on electromagnetic field analysis, such as FDTD or FEM, might result in a more accurate prediction of the electromagnetic environment in the LPS, but it also requires far more computer resources and a larger implementation time for the construction of each case setup than the method proposed in this paper. The idea of the proposed model is to offer a simple, feasible and fast alternative to electromagnetic field analysis which provides sufficient accuracy for practical purposes.

Declarations

Author contribution statement

Pablo Gomez: Conceived and designed the analysis; Analyzed and interpreted the data; Contributed analysis tools or data; Wrote the paper.

Funding statement

This research did not receive any specific grant from funding agencies in the public, commercial, or not-for-profit sectors.

Competing interest statement

The author declare no conflict of interest.

Additional information

No additional information is available for this paper.

 http://dx.doi.org/10.1016/j.heliyon.2016.e00178

References

[1] A. Sowa, Lightning overvoltages in wires within the buildings, International Symposium on Electromagnetic Compatibility, Cherry Hill, NJ, USA, 12–16 August, 1991, pp. 99–102.

[2] N. Fallah, C. Gomes, M.Z.A.A. Kadir, Lightning protection techniques for Roof-Top PV systems, International Power Engineering and Optimization Conference (PEOCO 2013), Langkawi, Malaysia, 3–4 June, 2013, pp. 417-–421.

[3] A. Sowa, Surge current distribution in building during a direct lightning stroke, International Symposium on Electromagnetic Compatibility, Cherry Hill, NJ, USA, 12–16 August, 1991, pp. 103–105.

[4] S. Wang, J. He, B. Zhang, R. Zeng, Time-domain simulation of small thin-wire structures above and buried in lossy ground using generalized modified mesh current method, IEEE Trans. Power Deliv. 26 (1) (2011) pp. 369, 377.

[5] J. Kato, H. Kawano, T. Tominaga, S. Kuramoto, Investigation of lightning surge current induced in reinforced concrete buildings by direct, International Symposium on Electromagnetic Compatibility, Montreal, Canada, 13–17 August, 2001, pp. 1009–1014.

[6] G. Maslowski, S. Wyderka, R. Ziemba, G. Karnas, K. Filik, L. Karpinski, Surge current distribution in the lightning protection system of a test house equipped in electrical and electronic appliances, 2014, International Conference on Lightning Protection (ICLP), Shanghai, China, 11–18 October, 2014, pp. 238–241.

[7] L. Li, V.A. Rakov, Distribution of currents in the lightning protective system of a residential building-part II: numerical modeling, IEEE Trans. Power Deliv. 23 (October (4)) (2008) 2447–2455.

[8] V. Hegde, V. Shivanand, On the characteristics of lightning currents in the steel reinforced concrete building due to a lightning strike, Asia-Pacific Symposium on Electromagnetic Compatibility (APEMC), Singapore, 21–24 May, 2012, pp. 865–868.

[9] R. Markowska, Lightning current distributions in LPS of a building with a radio base station on the roof, International Symposium on Electromagnetic Compatibility, Kyoto, Japan, 20–24 July, 2009, pp. 845–847.

[10] S. Miyazaki, M. Ishii, Role of steel frames of buildings for mitigation of lightning-induced magnetic fields, IEEE Trans. Electromagn. Compat. 50 (May (2)) (2008) 333–339.

 http://dx.doi.org/10.1016/j.heliyon.2016.e00178

[11] M. Ishii, K. Miyabe, A. Tatematsu, Induced voltages and currents on electrical wirings in building directly hit by lightning, Electr. Power Syst. Res. 85 (2012) 2–6.

[12] J. Chen, B. Zhou, F. Zhao, S. Qiu, Finite-difference time-domain analysis of the electromagnetic environment in a reinforced concrete structure when struck by lightning, IEEE Trans. Electromagn. Compat. 52 (November (4)) (2010) 914–920.

[13] A. Tatematsu, F. Rachidi, M. Rubinstein, Calculation of electromagnetic fields inside a building with layered reinforcing bar struck by lightning using the FDTD method, International Symposium on Electromagnetic Compatibility, Tokyo, Japan, 12–16 May, 2014, pp. 386–389.

[14] Y. Du, B. Li, M. Chen, Lightning-induced surges in building electrical systems, International Conference on Lightning Protection (ICLP 2014), Shanghai, China, 11–18 October, 2014, pp. 1217–1222.

[15] R. Liu, Y. Wang, Z. Zhao, Y. Zhang, Transient phenomena at point of strike for lightning strokes to concrete wall of building structures, International Conference on Lightning Protection (ICLP 2014), Shanghai, China, 11–18 October, 2014, pp. 1716–1719.

[16] R. Liu, Y. Wang, Z. Zhao, Y. Zhang, Magnetic field distribution inside metallic grid-like buildings struck by lightning based on finite element method, International Conference on Lightning Protection (ICLP 2014), Shanghai, China, 11–18 October, 2014, pp. 1712–1715.

[17] J.A. Gutierrez, P. Moreno, J.L. Naredo, J.L. Bermudez, M. Paolone, C.A. Nucci, F. Rachidi, Nonuniform transmission tower model for lightning transient studies, IEEE Trans. Power Deliv. 19 (April (2)) (2004) 490–496.

[18] P. Gómez, F.A. Uribe, The numerical Laplace transform: an accurate tool for analyzing electromagnetic transients on power system devices, Int. J. Electr. Power Energy Syst. 31 (February–March (2–3)) (2009) 116–123.

[19] J.A. Martinez-Velasco, A.I. Ramirez, M. Davila, In: J.A. Martinez-Velasco (Ed.), Overhead Lines in Power System Transients: Parameter Determination, CRC Press, Boca Raton, FL, 2009, pp. 23–28 Chapter 2.

[20] C. Gary, Approche Complete de la propagation multifilaire en haute frequence par utilization des matrices complexes, EdF Bulletin de la Direction des Etudes et Recherches (3/4) (1976) 5–20 ser. B.

[21] A. Deri, G. Tevan, A. Semlyen, A. Castanheira, The complex ground return plane a simplified model for homogeneous and multi-layer earth return, IEEE Trans. Power Apparatus Syst. PAS-100 (August (8)) (1981) 3686–3693.

 http://dx.doi.org/10.1016/j.heliyon.2016.e00178

[22] P. Gómez, P. Moreno, J.L. Naredo, Frequency domain transient analysis of non-uniform lines with incident field excitation, IEEE Trans. Power Deliv. 20 (July (3)) (2005) 2273–2280.

[23] P. Gómez, J.C. Escamilla, Frequency domain modeling of nonuniform multiconductor lines excited by indirect lightning, Int. J. Electr. Power Energy Syst. 45 (February (1)) (2013) 420–426.

[24] J.A. Martinez-Velasco, A. Ramirez, M. Davila, In: J.A. Martinez-Velasco (Ed.), Overhead Lines in Power System Transients: Parameter Determination, CRC Press, Boca Raton, FL, 2009, pp. 17–135.

[25] A. Morched, B. Gustavsen, M. Tartibi, A universal model for accurate calculation of electromagnetic transients on overhead lines and underground cables, IEEE Trans. Power Deliv. 14 (July (3)) (1999) 1032–1037.

[26] L. Bergeron, Water Hammer in Hydraulics and Waves Surge in Electricity, John Wiley, NY, 1961.

[27] T. Hara, O. Yamamoto, M. Hayashi, C. Uenosono, Empirical formulas of surge impedance for single and multiple vertical cylinder, Trans. IEE Jpn. E 110-B (February (2)) (1990) 129–136.

[28] A. Ametani, Y. Kasai, J. Sawada, A. Mochizuki, T. Yamada, Frequency-dependent impedance of vertical conductors and a multiconductor tower model, IEE Proc. Gener. Transm. Distrib. 141 (July (4)) (1994) 339–345.

[29] P. Gómez, Definition of a new formula for the characteristic impedance of vertical conductors for lightning transients, International Conference on Power Systems Transients (IPST 2015), Cavtat, Croatia, June, 2015.

 http://dx.doi.org/10.1016/j.heliyon.2016.e00178